

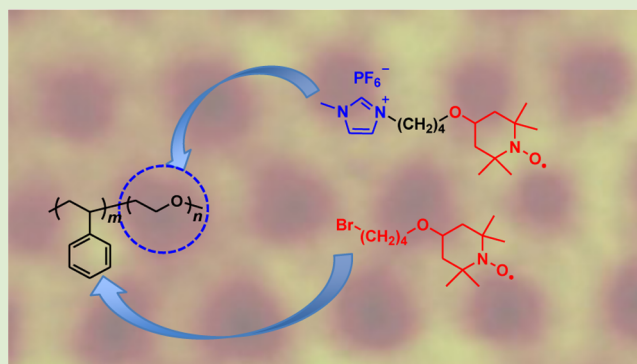
Ionic Liquid-Triggered Redox Molecule Placement in Block Copolymer Nanotemplates toward an Organic Resistive Memory

Takeo Suga,^{*,†} Kohei Aoki,[‡] and Hiroyuki Nishide^{*,‡}

[†]Waseda Institute for Advanced Study (WIAS) and [‡]Department of Applied Chemistry, Waseda University, Tokyo 169-8555, Japan

Supporting Information

ABSTRACT: The integration of functional components such as metal nanoparticles, metal salts, or ionic liquids with well-defined block copolymer (BCP) nanotemplates via non-covalent bond interactions has afforded hybrid functional materials. Here, we designed an ionic liquid (IL)-functionalized redox-active TEMPO (2,2,6,6-tetramethylpiperidine-*N*-oxy) radical (*guest*), investigated phase-selective incorporation/ placement into *host* BCP nanostructured matrices, and established a rational approach to functionalize BCP templates. On-demand domain functionalization of poly(styrene-*b*-ethylene oxide) (PS-*b*-PEO) was triggered by ion–ionophore interaction, as verified by the suppression of PEO melting transition in DSC, and the swelling behavior of the PEO spherical domain in AFM, TEM, and X-ray scattering characterizations. The obtained BCP layer containing the redox-active TEMPO and IL was utilized as an active layer in the diode-structured memory device, which exhibited on/off resistive switching (on/off ratio >10³). Systematic placement of TEMPO and IL in the BCP spherical domain allowed for tuning of the switching characteristics and revealed that the formation of a discontinuous redox-active domain was critical for rewritable resistive switching.



Prompted by the significant progress in the precise control over size, shape, and long-range ordering of block copolymer (BCP) nanotemplates,^{1–3} many research groups have focused on the integration of functional components such as metal nanoparticles (NPs), metal salts, or ionic liquids (ILs) into BCP nanodomains to embed (or deliver) their functionality.^{4–7} The metal NPs selectively incorporated in each BCP domain or their interface have been investigated as hybrid materials for microelectronic and photonic applications.^{8–10} Amphiphilic BCP–salt (e.g., Li⁺) complex or –IL gels have been examined as polyelectrolytes with high ionic conductivity and mechanical durability,^{11–13} leading to their potential applications in organic gate dielectrics, actuators, batteries, and fuel cells.¹⁴ The key challenges in the design of such hybrid materials based on noncovalent bond interactions among functional components and BCP segments are to control the location and loading amount of functional components, yet retaining the well-defined phase morphologies. Hydrogen bonding interactions have been extensively examined as a class of domain-selective noncovalent bond interactions;^{15,16} however, these weak interactions are comparative to the BCP self-assembly and are not trivial to tune the balance of segregation strength. In this study, we focused on rather stronger “ion–ionophore interactions” between the ILs and the ionophilic BCP segment and utilized ILs as the phase-selective “carrier” to drag functional molecules into BCP nanodomains. The advantages of using organic components in place of inorganic components are design flexibility of the

functional groups, tunable compatibility, and facile integration to the polymeric matrices. We selected robust but redox-active organic molecules, in particular, 2,2,6,6-tetramethylpiperidinyl-*N*-oxyl TEMPO radical, as target functional components.

Based on reversible and rapid redox reactions between a TEMPO radical and the oxoammonium salt, the TEMPO-functionalized polymers have been demonstrated as rechargeable battery electrodes with extremely high power (full charging within a few seconds) and excellent cycle life (>1000 cycles).^{17–19} The superior charge-storage characteristics of TEMPO justify their potential use for transient charge storage or charge transport even in a thin solid device configuration. In the last few decades, many approaches have been proposed for organic nonvolatile memory application,^{20–22} for example, the use of polyimides with donor–acceptor units²³ and the hybrid of polymer/metal NPs.^{24,25} Previously, we have proposed the combination of redox-active TEMPO and BCPs, and the significance of tailoring BCP morphologies, such as spheres, cylinders, and lamellae to modulate charge transport through the radical/ion-containing BCP layer: (a) nonswitching behavior for lamellae in parallel orientation, (b) write-once and read-many-times (WORM) memory for cylindrical morphology, and (c) rewritable and nonvolatile memory

Received: July 10, 2015

Accepted: August 10, 2015

Published: August 11, 2015



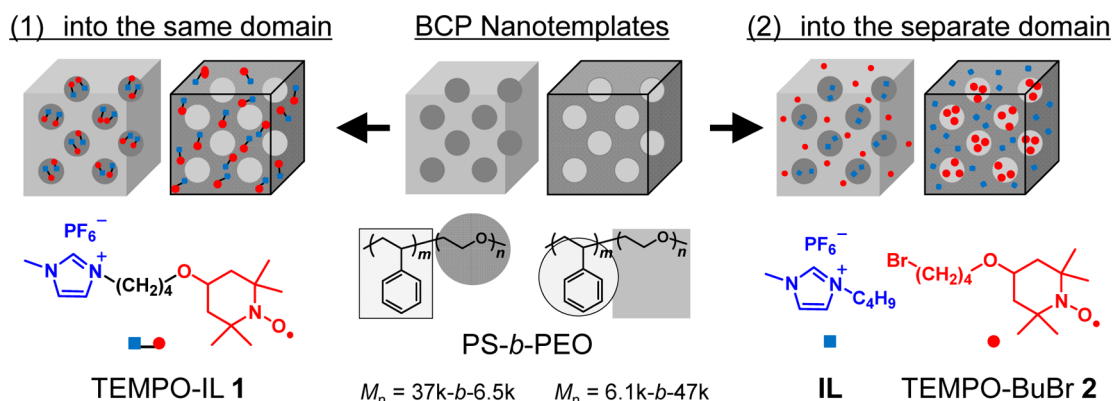


Figure 1. Preferential phase segregation of TEMPO-IL 1, TEMPO-BuBr 2, and IL (1-butylmethylimidazolium hexafluorophosphate) into spherical and inverse spherical PS-*b*-PEO(37–6.5), (6.1–47) nanotemplates.

characteristics for spherical domains.²⁶ Our initial findings for charge-transport modulation through functional BCP nanodomains (morphologies, orientation, and ordering) have a potential impact for the rational design of more efficient organic-based electronic devices. On the other hand, less attention has been paid to the role of the location/placement of individual functional groups (TEMPO and IL) in the BCP domains. In parallel (synthetic) approaches, we designed BCPs bearing (confining) TEMPO- and IL-segments and partially revealed the dominant effect of coexistence of TEMPO and IL on memory characteristics.²⁷ However, on-demand morphological tuning of the synthetic BCPs was not trivial. In this work, we focus on the spherical nanotemplate of conventional BCPs such as poly(styrene-*b*-ethylene oxide), PS-*b*-PEO, as a basic platform, and investigate the systematic placement of each functional group (TEMPO, ILs, and their conjugates) into BCP nanodomains via IL-triggered preferential phase segregation (Figure 1). Through the following careful morphological characterizations (DSC, AFM, TEM, and SAXS), we establish here ion–ionophore interaction as a viable strategy to functionalize BCP nanostructures and propose new insights on charge-transport modulation in the memory device.

We selected PS-*b*-PEO(37–6.5, PEO minor sphere) and (6.1–47, PS minor sphere), where the numbers in parentheses refer to the molecular weights of the PS and PEO blocks in kg mol^{-1} . The spherical (zero dimensional) domains can be easily close-packed and extended to 2D/3D stacks for memory cells without considering any alignment/orientation, which are often critical issues for cylindrical or lamellae morphologies.^{1,3} The TEMPO-substituted ionic liquid 1 and its precursor 2 were synthesized by a previously reported method.²⁶ Differential scanning calorimetry of PS-*b*-PEO(37–6.5)/1 and PS-*b*-PEO(37–6.5)/2 mixtures (5–50 wt % relative to the polymer) were performed to assess the miscibility of PS-*b*-PEO and 1 (or 2). Upon the addition of only 5 wt % of 1 and subsequent thermal annealing at 120 °C, the melting peak (T_m) for the PEO crystalline domain at 51 °C was clearly suppressed, indicating a dramatic reduction in the PEO crystallinity (Figure 2a). However, the addition of 2 did not affect the T_m for the PEO domain (Figure 2b). The glass transition temperature (T_g) of the PS domain in the vicinity of 100 °C was unchanged with an increase in the amount of 1, but slightly decreased with an increase in the amount of 2, which indicated that the TEMPO derivatives without the IL moiety preferentially plasticized the PS domain. The DSC diagram of PS-*b*-PEO containing the conventional IL, 1-butylmethylimidazolium

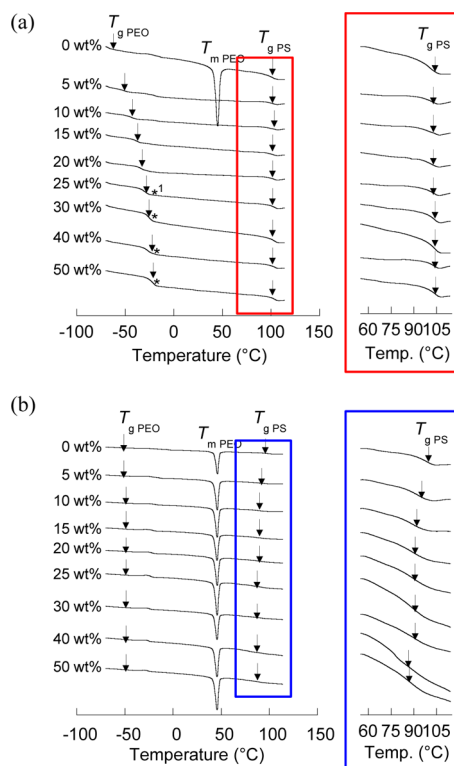


Figure 2. DSC diagram for the PS-*b*-PEO(37–6.5) film containing 0–50 wt % of (a) 1 and (b) 2 after thermal annealing (120 °C, 6 h). The additional peaks (*1) at higher loading amount (>25 wt %) were assigned to the thermal transition of the additive 1, respectively.

hexafluorophosphate, also showed a suppression of T_m peak of the PEO domain (Figure S1a), thus, supporting the role of the IL moiety as a predominant carrier that drags the TEMPO molecule into the PEO domain. The T_g of the PEO domain at –62 °C shifted to rather a higher value with the addition of 1, unlike the case of solvent-like swelling with IL, which suggested electrostatic physical association between the PEO segments and 1. Upon addition of higher loading amount (>25 wt %) of 1, a small additional peak ascribed to the thermal transition of 1 itself (Figure S1b) appeared in the vicinity of –20 °C in Figure 2a, which suggested less than 25 wt % addition of 1 would be the limit to retain the original spherical morphology.

Domain-selective functionalization of PS-*b*-PEO matrices with 1 or 2 was also characterized by morphological studies

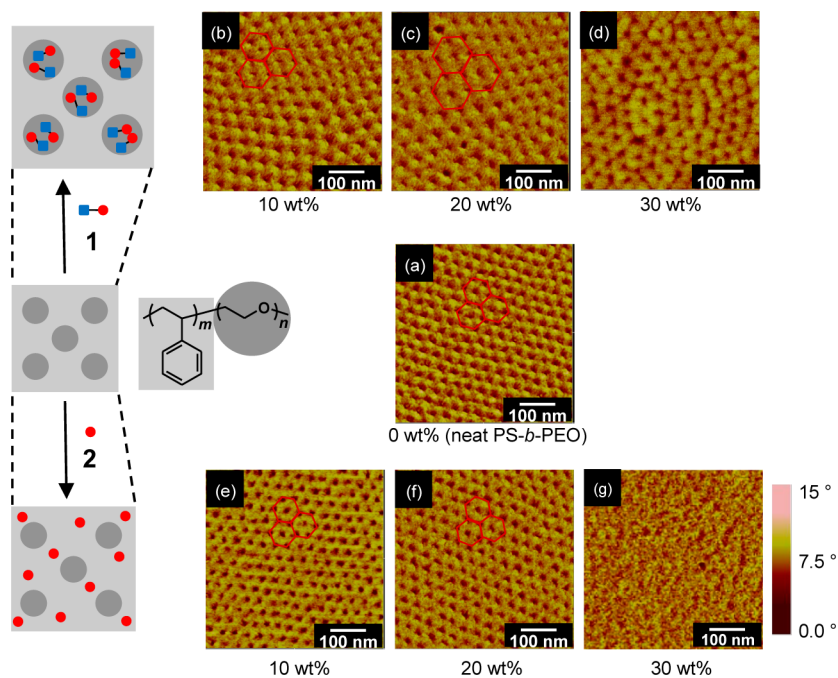


Figure 3. AFM phase images for (a) neat PS-*b*-PEO(37–6.5), (b–d) PS-*b*-PEO(37–6.5) containing 10, 20, and 30 wt % of **1**, and (e–g) PS-*b*-PEO containing 10, 20, and 30 wt % of **2**.

using atomic force microscopy (AFM, Figure 3) and transmission electron microscopy (TEM, Figure S2). A PS-*b*-PEO thin film containing 10–20 wt % of **1** was prepared on a silicon substrate via spin coating (100 nm in thickness), followed by solvent annealing under benzene vapors for 12 h. AFM phase images of neat PS-*b*-PEO(37–6.5) exhibited a hexagonally packed spherical morphology, where the PEO segments form minor spherical domains (Figure 3a). The size of the spherical domain increased from 18 to 26 nm as compared with that for the neat PS-*b*-PEO thin film, and the center-to-center distances between the PEO domains increased from 36 to 51 nm by the addition of **1** (Figure 3b,c, detailed values are summarized in Table 1). The significant change in the size of PEO spheres and the center-to-center distance can be ascribed to the crystalline-to-amorphous transition of the PEO domain by swelling. On the other hand, the addition of **2** did not induce any significant changes in the PEO domain size and center-to-center distance, indicating the placement of **2** in the free volume of the

amorphous PS domain (Figure 3e,f). Higher loading amount (>20 wt %) of **1** or **2** partially induced spherical-to-cylindrical phase transition and lowered the long-range ordering (Figure 3d,g). Thus, PS-*b*-PEO with the loading amount of <20 wt % was applied to retain the spherical morphology in the following section (device fabrication).

Grazing incidence small-angle X-ray scattering (GI-SAXS) was used to determine the morphologies and domain spacing of neat PS-*b*-PEO(37–6.5), PS-*b*-PEO/**1**, or PS-*b*-PEO/**2** blend films. The scattered intensity profiles as a function of the scattering vector q show three peaks at $1q^*$, $3^{1/2}q^*$, and $7^{1/2}q^*$, indicating a hexagonal arrangement of the spherical microdomains (Figure 4). The change in the center-to-center distances between the PEO spheres upon the addition of **1** or **2**, estimated from the primary scattering vector, q^* , was in good agreement with the measured AFM length scales (Table 1). As the concentration of **1** increased from 0 to 20 wt %, the

Table 1. Domain Size Change of PS-*b*-PEO(37-6.5) by Addition of **1** or **2**

additive	wt %	PEO domain size ^a (nm)	center-to-center distance ^a (nm)	center-to-center distance ^b (nm)
1	0	18.0 ± 2.0	36.1 ± 0.2	37.8
	5	19.4 ± 2.0	43.2 ± 1.0	
	10	23.7 ± 3.0	49.0 ± 2.1	44.5
	15	24.5 ± 3.5	50.3 ± 1.5	
	20	25.6 ± 3.5	50.5 ± 2.7	45.6
2	0	18.0 ± 2.0	36.1 ± 0.2	37.8
	5	17.7 ± 2.0	36.1 ± 0.2	
	10	17.8 ± 3.0	37.0 ± 0.6	38.0
	15	17.4 ± 2.5	35.5 ± 1.0	
	20	18.0 ± 2.5	37.7 ± 0.9	38.4

^aAnalyzed using AFM phase images (50 counts). ^bCalcd from q^* in GI-SAXS measurement.

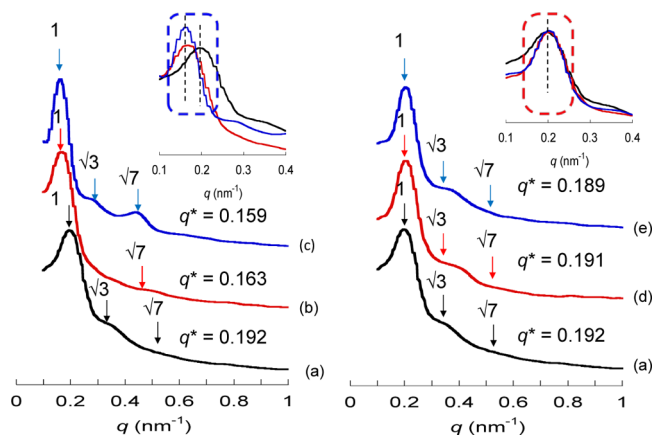
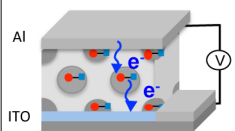
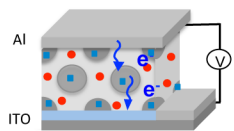
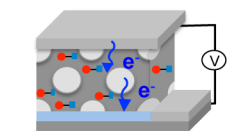
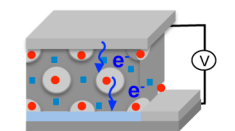


Figure 4. GI-SAXS profiles of PS-*b*-PEO(37–6.5): (a) neat PS-*b*-PEO, (b, c) containing 10 and 20 wt % of **1**, (d, e) containing 10 and 20 wt % of **2**. Inset: Magnified figures near the q^* region.

Table 2. Device Configuration and Memory Characteristics

	(a) Device I	(b) Device II	(c) Device III	(d) Device IV
Device configuration				
BCP templates	PS- <i>b</i> -PEO(37 – 6.5)	PS- <i>b</i> -PEO(37 – 6.5)	PS- <i>b</i> -PEO(6.1-47)	PS- <i>b</i> -PEO(6.1-47)
Guest	1 (20 wt%)	2 (20 wt%), IL (20 wt%)	1 (20wt%)	2 (20 wt%), IL (20 wt%)
TEMPO derivatives	discontinuous	continuous	continuous	discontinuous
IL domain	discontinuous	discontinuous	continuous	continuous
Memory characteristics	rewritable	WORM	WORM	rewritable

primary scattering peak q^* shifted to smaller q values (larger domain spacing). The volume change estimated from the domain spacing, $d = 2\pi/q^*$, was 163 and 176% for 10 and 20 wt % addition of **1**, respectively, which resulted from not only the added volume of **1** itself, but also the depression of PEO crystallites and PEO chain stretching by the incorporation of **1** into the PEO spheres. On the other hand, the primary q^* for the PS-*b*-PEO/**2** blend film was unchanged upon the addition of **2**, which can be ascribed to the preferential segregation of **2** into the free volume of the PS amorphous matrix.

The diode-structured thin film devices were fabricated with the mixed layer of PS-*b*-PEO(37–6.5) and PS-*b*-PEO(6.1–47) containing 20 wt % of **1** (devices I and III) or PS-*b*-PEO(37–6.5) and PS-*b*-PEO(6.1–47) containing both 20 wt % of **2** and **IL** (devices II and IV). Morphological characterizations for PS-*b*-PEO(6.1–47) containing **1** or **2** were shown in Figures S3 and S4 in detail. The block copolymer layer (ca. 150 nm in thickness) was prepared by spin-coating a 10 wt % THF solution on an ITO/glass substrate, followed by solvent annealing under benzene vapors. An aluminum top electrode was deposited by thermal evaporation under vacuum to give the monolayered device.

The typical I – V characteristics of the fabricated devices are summarized in Table 2. Upon application of the bias in the negative direction (0 to –5 V), device I comprising PS-*b*-PEO(37–6.5) and **1** (both TEMPO and IL moieties are incorporated into the same PEO minor spheres) exhibited a drastic current density increase (on state) at about –3 V as the threshold voltage (on/off ratio $>10^3$; Figure S6). Upon application of the positive bias (0 to +5 V), the device was switched back to the high resistance (off) state at +2.2 V. The repeatable on/off switching of the device I was verified over more than 3000 cycles. Device II comprising PS-*b*-PEO(37–6.5) containing **2** and **IL** in separate domains also exhibited resistive switching behavior (on/off ratio $>10^4$), but it was irreversible (write-once-read-many times, WORM; Figure 5). Our earlier work on the device utilizing a synthesized AB block copolymer bearing TEMPO and imidazolium groups at separate segments also exhibited the same WORM behavior.²⁷ Thus, we anticipated that the coexistence of TEMPO and IL in the same domain would be the requisite for repeatable on/off switching.

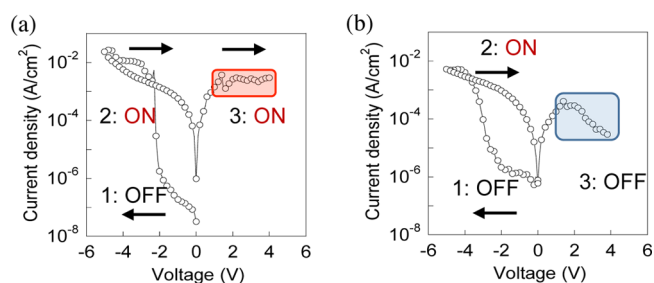


Figure 5. I – V characteristics for devices II and IV. Black arrows with numbers indicate the programmed voltage cycle.

We also investigated the case of inverse spherical domains (PS sphere) using PS-*b*-PEO(6.1–47). Device III containing **1** exhibited WORM behavior (Table 2, inset and Figures S6 and 7a), as in the case of the cylindrical morphology with a continuous PEO phase containing both TEMPO and IL, connecting two electrodes.²⁶ On the other hand, device IV, in which **2** and **IL** are located in separate domains, interestingly exhibited repeatable on/off switching behavior, which was initially unexpected (Figures 5 and S7b). As highlighted in Table 2, the memory characteristics was tuned by adjusting the location of the functional groups (TEMPO, IL, and their conjugates). In particular, the location and discontinuity of the TEMPO domains played a more critical role in realizing repeatable on/off switching (rewritable memory devices) rather than coexistence of TEMPO and IL. The repeatable on/off switching of the device IV was also verified over more than 3000 cycles (Figure S7b).

In summary, the ion–ionophore interaction between IL and ionophilic BCP nanodomains was utilized for preferential phase segregation of functional molecules, especially the redox-active TEMPO. Precise control of the location and loading amount of TEMPO, IL, and their conjugates yielded a wide range of functional domains on-demand. We proposed and established here ionic liquid-triggered placement of a functional molecule as a rational design approach for functional BCP nanodomains. The diode-structured device sandwiching the obtained functional BCP layer with spherical morphology exhibited on/off resistive switching ($>10^3$), and the rewritability of the memory device was tunable with the location of functional groups such as the discontinuous redox-active domain. The results here

demonstrated the high impact to combine/multiply the functionality of the embedded molecules and morphological diversity. Our systematic, on-demand functionalization approach successfully integrated with the well-defined BCP nanotemplates can provide good model to elucidate the origin/requisite for redox-based, charge-transport modulation in organic electronic devices. In situ conductive AFM analysis is ongoing and will be reported in future studies.

■ ASSOCIATED CONTENT

■ Supporting Information

Experimental details. DSC diagram for PS-*b*-PEO(37–6.5) containing conventional **1L** (0–50 wt %) and **1** itself. TEM images of PS-*b*-PEO containing **1** or **2**. DSC diagram and TEM images for PS-*b*-PEO(6.1–47) (inverse spherical morphology) containing **1** or **2**. Line-cut profile of AFM images. DSC diagram and TEM images for PS-*b*-PEO(6.1–47) containing **1** or **2**. *I*–*V* characteristics of the devices **I** and **III**. Cycle and retention tests of the devices **II** and **IV**. The Supporting Information is available free of charge on the ACS Publications website at DOI: 10.1021/acsmacrolett.5b00473.

(PDF)

■ AUTHOR INFORMATION

Corresponding Authors

*E-mail: takeosuga@toki.waseda.jp.

*E-mail: nishide@waseda.jp.

Notes

The authors declare no competing financial interest.

■ ACKNOWLEDGMENTS

This work was partially supported by Grants-in Aid for Scientific Research (Nos. 24225003 and 23550139) from MEXT, Japan. T.S. acknowledges the MEXT/JST tenure-track program, Grants-in Aid for Scientific Research on Innovative Areas on New Polymeric Materials Based on Element-Blocks (Nos. 25102541 and 15H00766), and the MIZUHO Foundation.

■ REFERENCES

- (1) Kim, H.-C.; Park, S.-M.; Hinsberg, W. D. *Chem. Rev.* **2010**, *110*, 146.
- (2) Bang, J.; Jeong, U.; Ryu, D.-Y.; Russell, T. P.; Hawker, C. J. *Adv. Mater.* **2009**, *21*, 4769.
- (3) Bates, C. M.; Maher, M. J.; Janes, D. W.; Ellison, C. J.; Willson, C. G. *Macromolecules* **2014**, *47*, 2.
- (4) Bockstaller, M. R.; Mickiewicz, R. A.; Thomas, E. L. *Adv. Mater.* **2005**, *17*, 1331.
- (5) Nunns, A.; Gwyther, J.; Manners, I. *Polymer* **2013**, *54*, 1269.
- (6) Lodge, T. P. *Science* **2008**, *321*, 50.
- (7) Ueki, T.; Watanabe, M. *Macromolecules* **2008**, *41*, 3739.
- (8) Zhao, Y.; Thorkelsson, K.; Mastroianni, A. J.; Schilling, T.; Luther, J. M.; Rancatore, B. J.; Matsunaga, K.; Jinnai, H.; Wu, Y.; Poulsen, D.; Frechet, J. M. J.; Alivisatos, A. P.; Xu, T. *Nat. Mater.* **2009**, *8*, 979.
- (9) Lin, Y.; Daga, V. K.; Anderson, E. R.; Gido, S. P.; Watkins, J. J. *J. Am. Chem. Soc.* **2011**, *133*, 6513.
- (10) Son, J. G.; Bae, W. K.; Kang, H.; Nealey, P. F.; Char, K. *ACS Nano* **2009**, *3*, 3927.
- (11) Kim, S. H.; Misner, M. J.; Yang, L.; Gang, O.; Ocko, B. M.; Russell, T. P. *Macromolecules* **2006**, *39*, 8473.
- (12) Young, W.-S.; Epps, T. H. *Macromolecules* **2009**, *42*, 2672.
- (13) Virgili, J. M.; Hoarfrost, M. L.; Segalman, R. A. *Macromolecules* **2010**, *43*, 5417.

(14) Cho, J. H.; Lee, J.; He, Y.; Kim, B.-S.; Lodge, T. P.; Frisbie, C. D. *Adv. Mater.* **2008**, *20*, 686.

(15) Tang, C.; Lennon, E. M.; Fredrickson, G. H.; Kramer, E. J.; Hawker, C. J. *Science* **2008**, *322*, 429.

(16) Matsushita, Y. *Macromolecules* **2007**, *40*, 771.

(17) Nishide, H.; Oyaizu, K. *Science* **2008**, *319*, 737.

(18) Suga, T.; Ohshiro, H.; Sugita, S.; Oyaizu, K.; Nishide, H. *Adv. Mater.* **2009**, *21*, 1627.

(19) Suga, T.; Sugita, S.; Ohshiro, H.; Oyaizu, K.; Nishide, H. *Adv. Mater.* **2011**, *23*, 751.

(20) Lin, W.-P.; Liu, S.-J.; Gong, T.; Zhao, Q.; Huang, W. *Adv. Mater.* **2014**, *26*, 570.

(21) Ling, Q. D.; Liaw, D. J.; Zhu, C. X.; Chan, D. S. H.; Kang, E. T.; Neoh, K. G. *Prog. Polym. Sci.* **2008**, *33*, 917.

(22) Scott, J. C.; Bozano, L. D. *Adv. Mater.* **2007**, *19*, 1452.

(23) Kurosawa, T.; Higashihara, T.; Ueda, M. *Polym. Chem.* **2013**, *4*, 16.

(24) Leong, W. L.; Lee, P. S.; Lohani, A.; Lam, Y. M.; Chen, T.; Zhang, S.; Dodabalapur, A.; Mhaisalkar, S. G. *Adv. Mater.* **2008**, *20*, 2325.

(25) De Rosa, C.; Auriemma, F.; Girolamo, R. D.; Pepe, G. P.; Napolitano, T.; Scalfaferrri, R. *Adv. Mater.* **2010**, *22*, 5414.

(26) Suga, T.; Takeuchi, S.; Nishide, H. *Adv. Mater.* **2011**, *23*, 5545.

(27) Suga, T.; Sakata, M.; Aoki, K.; Nishide, H. *ACS Macro Lett.* **2014**, *3*, 703.